

# Single photon sensitive Geiger-mode LADAR cameras

Ping Yuan<sup>\*</sup>, Rengarajan Sudharsanan, Xiaogang Bai, Paul McDonald, and Eduardo Labios

Spectrolab Inc., a Boeing Company, 12500 Gladstone Ave., Sylmar, CA, USA 91342

Bryan Morris, John P Nicholson, Gary M Stuart, and Harrison Danny  
Boeing DES, 4411 The 25 Way NE # 350, Albuquerque, NM 87109

## ABSTRACT

Three-dimensional (3D) imaging with Short wavelength infrared (SWIR) Laser Detection and Range (LADAR) systems have been successfully demonstrated on various platforms. It has been quickly adopted in many military and civilian applications. In order to minimize the LADAR system size, weight, and power (SWAP), it is highly desirable to maximize the camera sensitivity. Recently Spectrolab has demonstrated a compact 32x32 LADAR camera with single photo-level sensitivity at 1064. This camera has many special features such as non-uniform bias correction, variable range gate width from 2 microseconds to 6 microseconds, windowing for smaller arrays, and short pixel protection. Boeing integrated this camera with a 1.06  $\mu\text{m}$  pulse laser on various platforms and demonstrated 3D imaging. The features and recent test results of the 32x128 camera under development will be introduced.

## 1. INTRODUCTION AND BACKGROUND

SWIR 3D imaging provides one more important dimension in foliage penetration, camouflage imaging, and aerial mapping in battlefield intelligence and earth survey. The potential market for its airborne applications is greatly influenced by the size, weight, and power (SWAP) of LADAR systems. Since the laser and its service system takes most of the system SWAP, it is essential to maximize the camera sensitivity to reduce the laser power in order to enhance the ranging distance and reduce the SWAP of the whole system. By reaching the optical detection quantum limit, InP-based single-photon counting Geiger-mode avalanche photodiodes (GM-APD) fit perfectly to this requirement. SWIR GM-APD focal plane arrays (GM-FPAs) have been reported by both MIT Lincoln Laboratory<sup>1</sup> and Boeing Spectrolab<sup>2</sup>. Due to the availability of high power emitters, most of the effort to date has been focused on photodiodes operating at 1.06  $\mu\text{m}$ .

Important figures of merits for GM-APDs include dark count rate (DCR) and photon detection efficiency (PDE) which together establish the upper limit of the signal-to-noise ratio for the camera. For active 3D imaging, the upper limit of range resolution is determined by FPA timing jitter, while the spatial resolution is largely determined by FPA crosstalk. Frame rate describes how often the camera can take a 3D shot. Because GM-APD cameras normally require multiple frames to get clear pictures, and this parameter will greatly influence the aircraft speed and survey efficiency. Since the frame rate is primarily determined by the data process and download rate, the GM-APD afterpulsing, or temporal crosstalk between range gates, is normally not a great concern in imaging applications as long as it is no less than 100 kHz. Other important parameters include weight, power, and volume. Because most of the power consumed in a LADAR camera is by the thermoelectric coolers (TEC), a higher APD operation temperature is highly desirable to airborne applications.

We have been improving the performance of both the avalanche photodiode detector and ROIC arrays that together comprise an FPA. The enhanced capabilities of the newly designed 32x32 ROIC include non-uniform bias (NUB) correction and short pixel protection. Instead of biasing the whole array with a single voltage in most focal plane arrays (FPA), NUB can tune the bias individually to pixels with 4-bit resolution

<sup>\*</sup> Email: [ping.yuan@boeing.com](mailto:ping.yuan@boeing.com); Tel: 818 898 7578; Fax : 818 838 7474.

and in a 2.5 V range. High voltage is applied to pixels to operate in Geiger mode. A single pixel shorting out of the thousands of pixels can reduce the array APD bias, overheat the local area, and cause an FPA failure. The short-related failure may occur in the array fabrication, FPA assembly, and later usage. In order to improve the FPA yield, uniformity, and reliability, the pixel input circuit was modified and effectively removed high dark current (shorted) APD pixels from the array to reduce the overall current draw of an APD array. Spectrolab has also introduced a feature to the APD detector array that reduces the optical crosstalk between pixels to <100ppm and reduces Dark Count Rate (DCR) at operating temperature to <10 kHz. External PDE on detectors alone, without a microlens, in excess of 40% has been demonstrated for reverse-illuminated arrays.

Parameter	Spec	Test conditions
Wavelength	1.06 $\mu\text{m}$	
Format	32x32	
Pixel Pitch	100 $\mu\text{m}$	
PDE	40%	240K, 4V overbias
Fill Factor	70%	
DCR	20 kHz	240K, 4V overbias
Cross talk	<1%	Optimized overbias for SCA
Pixel operability	99%	
RMS timing jitter	0.5 ns	

**Table 1.** Typical single photon counting focal plane array figures of merits for a 32x32 GM-APD array presently fabricated at Spectrolab.

All these parameters mentioned above must be optimized for the optimal sensor performance. In practice these parameters are not decoupled and often trade off against one another. Table 1 lists the most important FPA figures of merit that impact single photon counting sensor systems.

## 2. GM-APD DEVICE

In Geiger-mode operation the avalanche photodiodes are biased above the breakdown voltage,  $\sim 2\text{-}4\text{ V}$ , for a short period of time during which the sensor is active. Due to various carrier generation mechanisms in GM-APDs, there is some probability for the pixels to generate some output pulses even without any incident photons. This probability is characterized by dark count rate (DCR) and it represents the noise of GM-APD arrays. The maximum length of this active period is also determined by DCR. If a photon in the sensitive spectrum falls on the detector pixel in this period, it has a probability to be absorbed and multiplied in the GM-APD such that the amplitude of the result pulse is large enough to be converted into a digital pulse that can be registered by the following readout circuit. This probability is a figure of merit called photon detection efficiency (PDE).

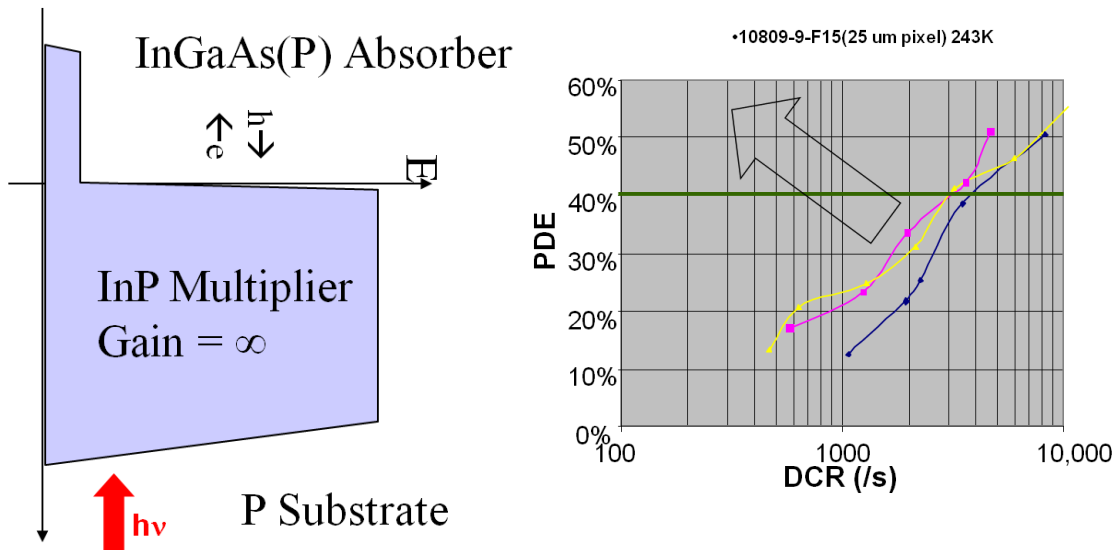


**Figure 1** The electric field profile during operation Geiger-mode operation of an APD. The right panel shows PDE as function of DCR of three typical Spectrolab 25- $\mu\text{m}$  diameter Geiger-mode APD pixels of a 32x128 array. The data are measured at various overbias points and at 243 K.

In order to suppress the dark current generation in the narrow band absorber and achieve high gain in the multiplier, the InGaAsP/InP GM-APD separate absorption and gain and multiplication (SAGM) device structure is tuned for 1.06  $\mu\text{m}$  operation and the electric field profile is shown in Figure 1. An InGaAsP alloy is used in the absorption layer for 1.06- $\mu\text{m}$  photons. DCR increases with overbias and operating temperature. Because a higher overbias also yields a better PDE, for a better signal-to-noise ratio, the trade-off between PDE and DCR has to be carefully considered in the device operation point selection. The right panel plots the PDE against DCR of three 25- $\mu\text{m}$  array pixels on a 32x128 GM APD array under different overbiases and at 243K. Grown on p-type InP substrates, the devices can achieve 40% PDE with 3~4 kHz DCR at the operation temperature.

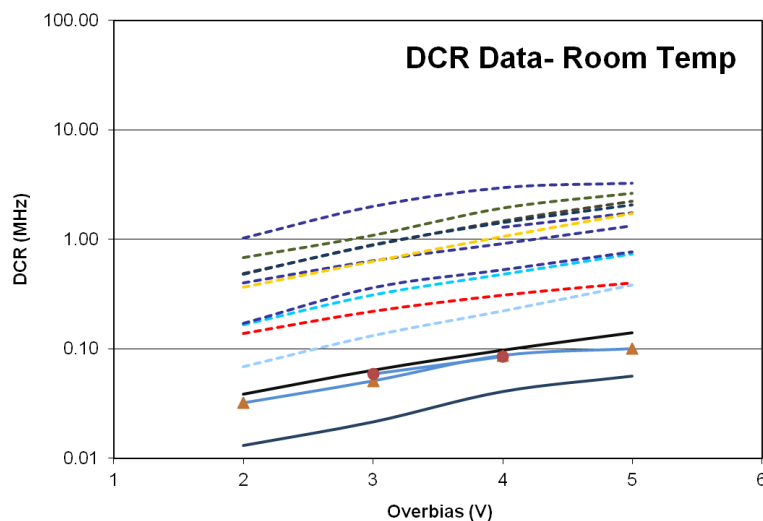


**Figure 2** The DCR vs overbias plots of Spectrolab 30- $\mu\text{m}$  GM-APDs at room temperature through generations. The devices grown on N+ InP substrates are shown in dotted lines. The devices grown on P+ InP substrates are shown in solid lines. The latest GM-APDs on P- InP substrates are shown in solid lines with symbols. Over the years, the device DCR was reduced by about two orders of magnitudes.

The GM-APD performance improvement at Spectrolab is shown in Figure 2 and Figure 3. Figure 2 illustrates the DCR improvement of Spectrolab 30- $\mu\text{m}$  GM-APDs at room temperature through generations. By changing to P InP substrates and optimizing the growth condition and device process<sup>2,3</sup>, the bottom parasitic forward-biasing pn junction was eliminated and the DCR was reduced by about two orders of magnitude. The P- InP substrate also helps to reduce the substrate free carrier absorption and improve the DCR-PDE tradeoff. Coupled with the ROIC optimization in the same time, the resulted SCA improvement is visualized in Figure 3. Obviously, both sensor uniformity and noise are greatly improved.

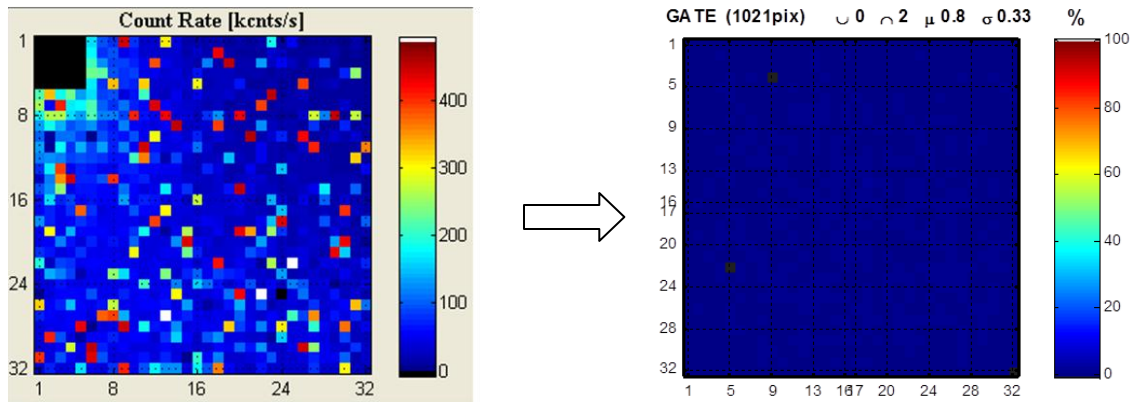


**Figure 3** The improvement in DCR map of 32x32 LADAR cameras. The left panel shows an SCA with an GM-APD array on N+ InP substrate with a CMOS 2002 ROIC. Both the mean DCR and hot pixel counts are high. The right panel shows the DCR map of a recent SCA with P-InP substrate APD array and a new 32x32 ROIC in a Spectrolab GenII LADAR camera. The DCR mean is about 0.8 kHz with a standard deviation of 0.33 kHz.

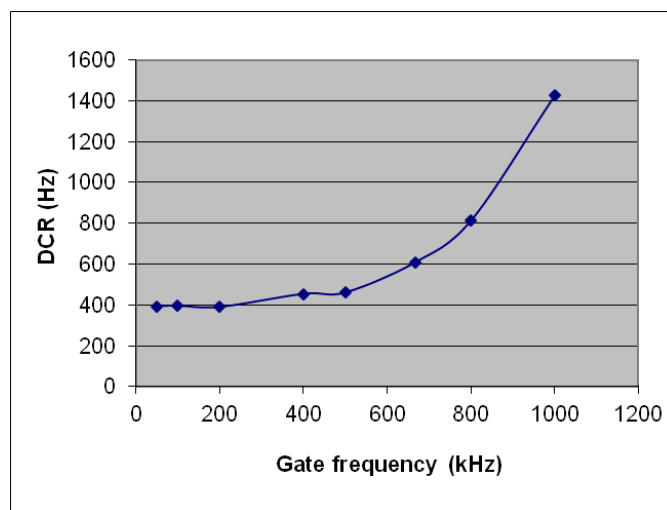


**Figure 4** The afterpulsing induced DCR rise. It is measured at 243 K and 4 V overbias with a 30  $\mu\text{m}$  pixel and 20 ns gate. At the low gate frequencies, the DCR is about 400 Hz. The afterpulsing effect has little impact until about 500 kHz gate frequency, which is far beyond the normal camera frame rate.

For better electric field control, a mesa structure is employed for the array pixels. Due to the natural optical medium discontinuity in the sensor plane, the crosstalk due to the lateral optical propagation suffered by planar structures is greatly suppressed, and no isolation trench is necessary. Also because of the absence of the trenches and guard rings for the planar structures, the potential for smaller pixel pitch and larger fill factor is only limited by the dimension of the mesa separations, which can be easily restricted to a few microns. After pulsing has been a concern for Geiger-mode APDs. In each avalanche event, a large amount of carriers are generated and transported through the APD junction. Some carriers will be trapped in the hetero-interfaces and trapping defects. As released later, they may trigger a false alarm and result in a higher dark count rate if the operation cycle is shorter than or comparable to the trap lifetime. This after pulsing will deteriorate at the reduced temperature, at which GM-APDs normally operate. By depleting all the active regions, the mesa structure will avoid the time consuming carrier detrapping-diffusion-collection process in weak electric field, and reliably suppress the after pulsing effect.

One way to characterize this afterpulsing effect is to measure the DCR at different gate frequencies. Comparing to the planar APD structures, the mesa pixels in our array fully deplete the absorber and multiplier in the whole operation cycle and avoid the long trapping time of the photo- or avalanche-generated carriers in weak electric field. As shown in Figure 4, a typical 30  $\mu\text{m}$  pixel was measured at 243 K, 4 V overbias, and 20 ns gate. At the low gate frequencies, the DCR is about 400 Hz. The afterpulsing effect has little impact until the gate frequency is about 500 kHz, which is far beyond the normal camera frame rate.

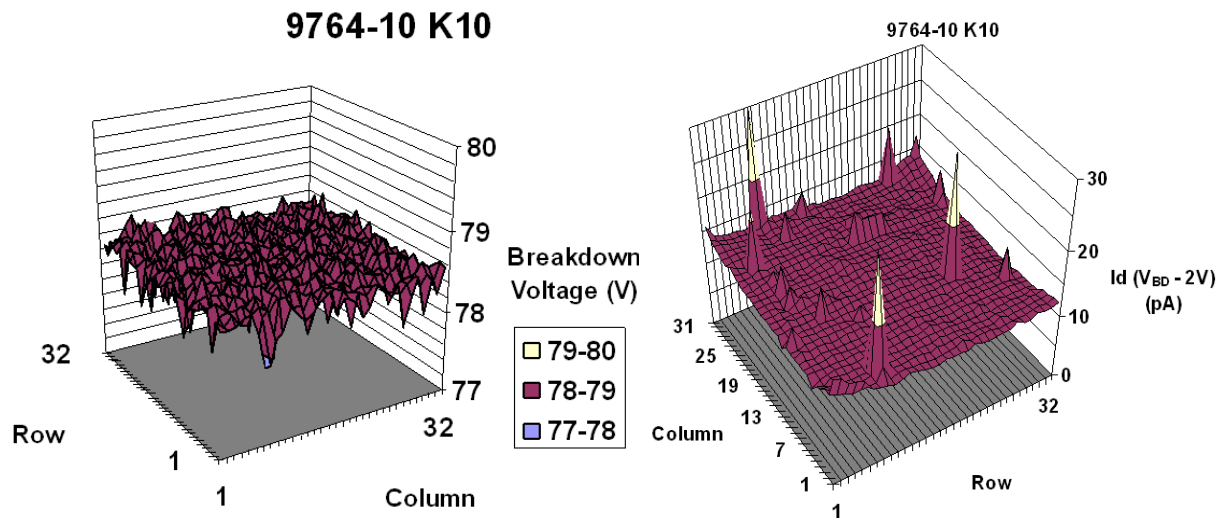


**Figure 5** The breakdown voltage ( $V_{br}$ ) and dark current ( $I_d$ ) map of a typical 32x32 GmAPD array. The median  $V_{br}$  is 78.5V and the standard deviation is 0.16V in the left panel. The dark current median is 12.3 pA with a standard deviation of 3.7 pA.

Due to the epitaxial non-uniformity, normally there is a breakdown voltage ( $V_{br}$ ) variation across the array. For most FPA applications, the common anode is biased with a single negative voltage, while the pixels are applied a positive pulse uniformly in the detection gate. Under this bias scheme, the overbias to each pixel will vary with the breakdown voltage and result in non-uniformity in DCR and PDE. For uniform performance, it is critical to minimize the  $V_{br}$  variation across the array. Figure 5 shows the  $V_{br}$  and  $I_d$  maps of a typical 32x32 GmAPD array. The standard deviation of  $V_{br}$  is about 0.16 V, and that of  $I_d$  is 3.7 pA.

With extensive capacities in MOVPE epitaxy, wafer process, and module packaging, Spectrolab vertically integrated the LADAR camera manufacturing in house. After the detector array fabrication, Indium bumps were evaporated on to the array pixels. The detector array was integrated with a ROIC of the same format

by flip-chip bonding. A GaP microlens array was attached to the focal plane array for a better fill factor afterward.

Figure 6 shows the cross section of a 32x128 SCA. The FPA and the interposer were mounted on to a TE cooler and the assembly was soldered in a 160-pin grid array package. Later, the package was hermetically sealed with an AR-coated sapphire window.

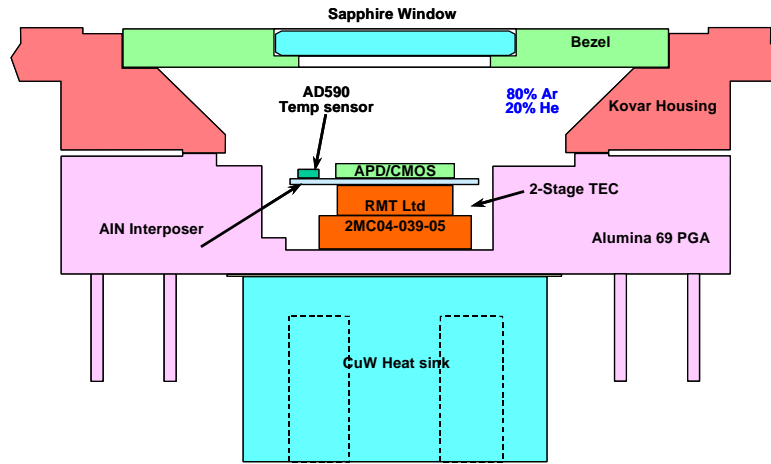


**Figure 6.** The cross section of a Spectrolab 32x128 SCA.

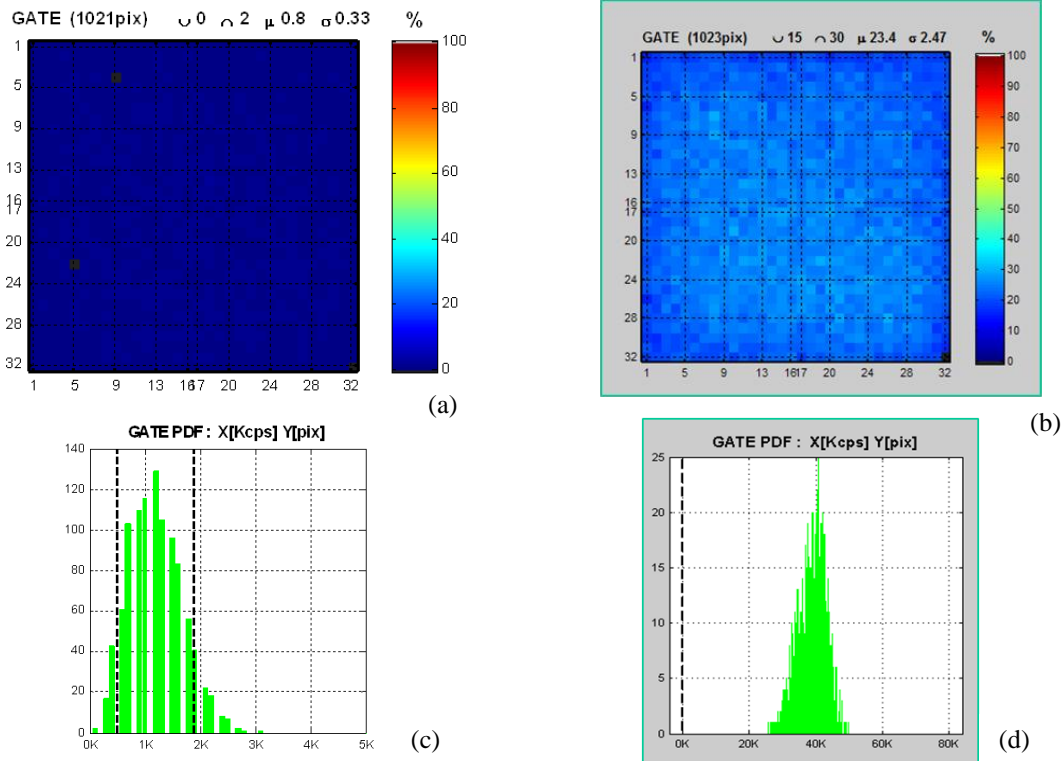


**Figure 7** The DCR and PDE uniformity of an SCA without NUB correction. In the operation condition, (a) shows the DCR map with a mean of 0.8 kHz and 0.33 kHz in standard deviation. (c) shows the corresponding DCR histogram. The PDE map shown in (b) is measured under the same operation condition with flood illumination. The mean count is 23.4 kHz with a standard deviation of 2.47 kHz.



### 3. SPECTOLAB GEN-II 32X32 LADAR CAMERA

With the support from DARPA, a 32x32 readout-integrated circuit (ROIC), BFE316, was designed in 180-nm CMOS technology by Black Forest Engineering (BFE). Many improvements were incorporated in this design based on our experience with the previous versions. They include: short pixel protection, 4-bit APD array NUB correction, 7  $\mu\text{s}$  gate width with 0.5 ns resolution (or 1000 m range with 7.5 cm resolution), 435-ps whole system jitter, negligible chirp, 14V max overbias, and 300 mW power consumption<sup>4</sup>.

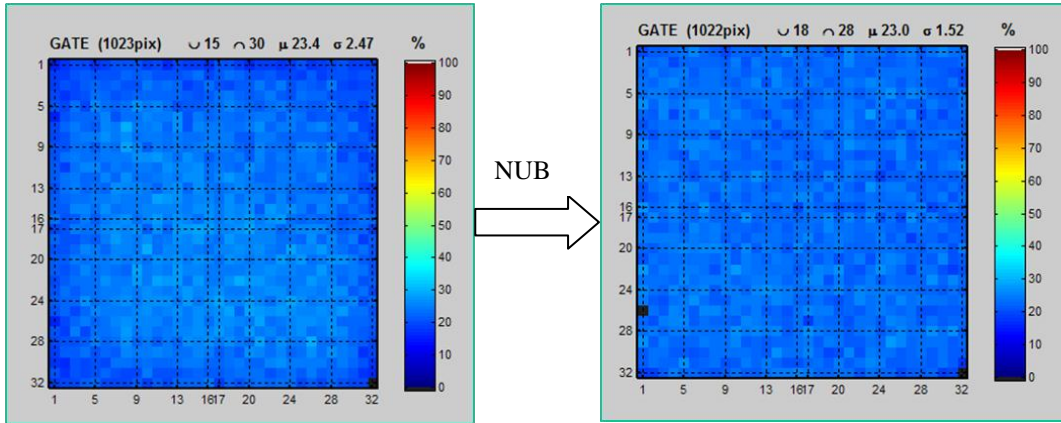


**Figure 8.** The PDE map of a 32x32 SCA operated at 242K and a frame rate of 12.5 kHz.

Uniformity is a critical array performance. As shown in Figure 5, APD arrays have natural variations in breakdown voltage, which results in a performance variation across the array if it is biased under a uniform bias. A lot of effort has been invested in its improvement in semiconductor growth, device process, and SCA assembly. Figure 7 shows the DCR and PDE maps and histogram of an SCA at the operation condition without NUB correction. In the operation condition, (a) shows the DCR map with a mean of 0.8 kHz and 0.33 kHz in standard deviation. (c) shows the corresponding DCR histogram. The PDE map shown in (b) is measured under the same operation condition with flood illumination. The mean count is 23.4 kHz with a standard deviation of 2.47 kHz. Because of the difficulty of the illumination calibration, the absolute PDE value of each pixel is not available from this SCA measurement. In applications its value is estimated with the device performance as shown in Figure 1.

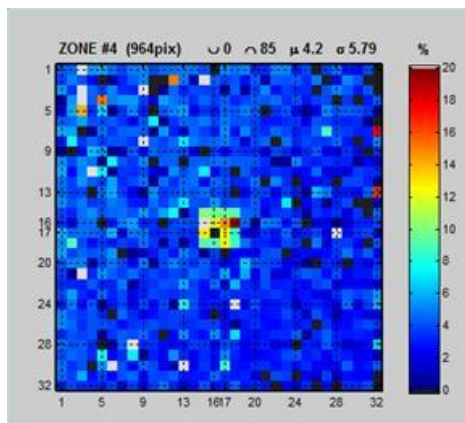


**Figure 9** Enhanced sensitivity in a 4x4 region near the array center realized with the NUB function.

By introducing a 4-bit 2.5V in-pixel programmable NUB adjustment, even better performance uniformity can be achieved. Figure 8 demonstrated the NUB improvement in PDE of the same SCA shown in Figure 7. With a tuning range of  $\pm 0.75V$  in the individual pixel bias and the PDE map, the NUB function reduced the photo count standard deviation from 2.47 kHz to 1.52 kHz, while keeping the photo count mean nearly unchanged. This function also allows array windowing: increased or decreased sensitivity within a specified region. Figure 9 demonstrated a 4x4 region with enhanced sensitivity near the array center. Working like a digital optical aperture, this windowing function can avoid the interference and cross talk from other pixels out of the target area.

Short pixel protection is another important feature implemented in this ROIC. With the immunity to sparse shorted detectors normally in APD arrays, this protection in the front end circuit greatly improves manufacturability and stability of FPAs.

The ROIC power consumption is reduced to 300 mW, about 50% of the previous version. Because the FPA is at the top of several stages of TECs, which consume most of the power in a LADAR camera, the nearly halved ROIC power consumption dramatically reduced the camera power load and heatsink weight.

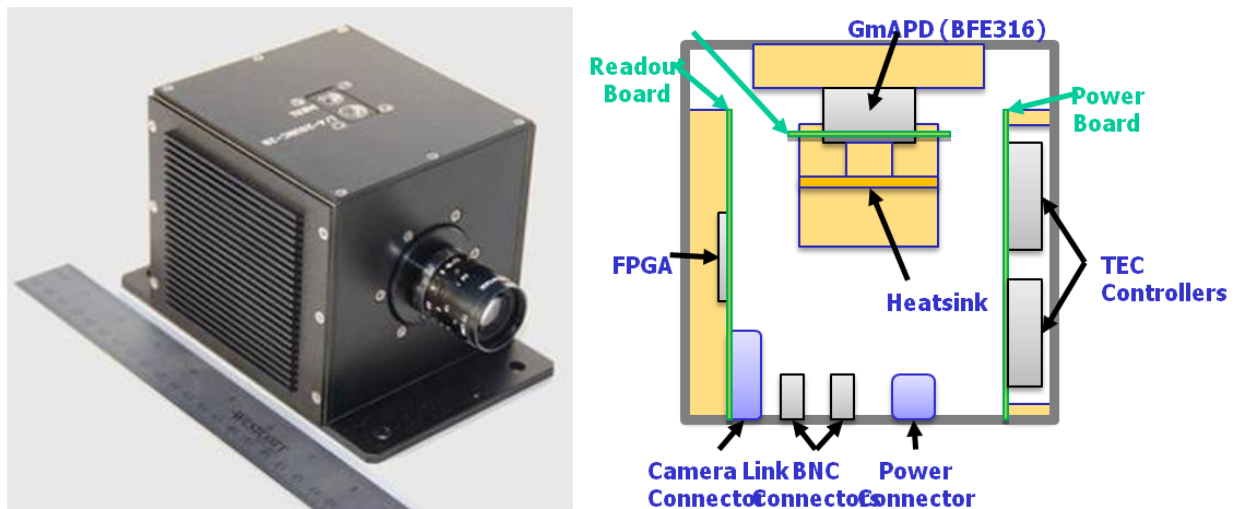


**Figure 10** Spectrolab Gen-II 32x32 GmAPD LADAR camera.

With the readout boards developed at Boeing DES, the Gen-II 32x32 LADAR camera was integrated with the SCA based on the BFE 316 ROIC. Figure 10 illustrates this camera and its internal structure. With GM APDs, the single photon level sensitivity greatly extends the LADAR system range, reduces the laser power requirements and the lens size, and minimizes the SWAP of the overall system. In Spectrolab Gen-II 32x32 LADAR camera, the detection gate can be kept on for about 7  $\mu s$ , which provides a range window of about 1 km long. Additional range coverage can be realized by inserting a delay between the laser pulse and gate turn-on and shifting the range window until reaching the maximum range allowed by the laser power and the array sensitivity. With a proper delay, the laser signal will fall in the detection gate and fire pixels in the array. The following circuits of the fired pixels will latch the timing of the detection. At the end of the gate, the whole array will be scanned and the timing information will be read out.

The ranging resolution of a LADAR camera is determined by its overall jitter and chirp performance. The temporal histogram of our Gen-II 32x32 camera to a synchronized 90 ps laser pulse is shown in the top panel of Figure 11. The bin size is 500 ps, and the laser pulse width is included in this measurement. By calculating the standard deviation of this temporal distribution, we can get the overall system RMS jitter of 418 ps, which includes the laser pulse width and jitters in the trigger loop, APDs, ROIC, and readout boards and is shorter than the 500ps bin size. With a new clock design, the chirp in this camera is



negligible. As shown in the bottom panel of Figure 11, by increasing the delay of a laser pulse 500 ns each time, we have got a series of evenly spaced signals in the detection gate.

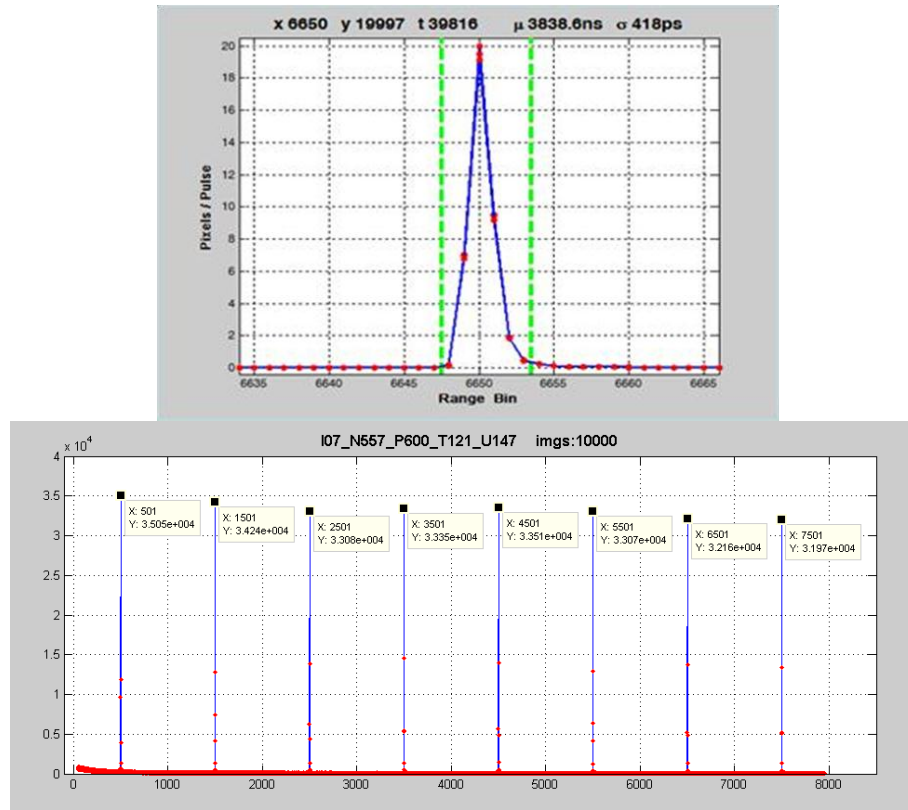


**Figure 11** The top graph shows the temporal histogram of a single laser pulse detected by a Spectrolab Gen-II 32x32 LADAR camera. The overall system RMS jitter is about 418 ps. The bottom panel shows a series of signals detected from laser pulses delayed by 500 ns from each other.

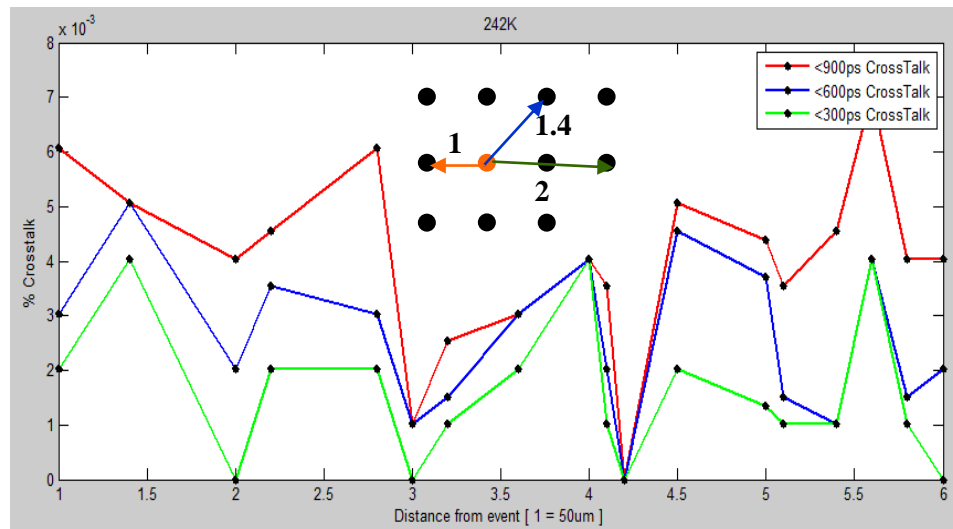


**Figure 12** The crosstalk probability as a function of the distance to the initiating pixel. The pixel distance used in the x-axis is illustrated in the inserted diagram.

Because the GM APDs are biased beyond the breakdown voltage and they are extremely sensitive to single photon level in the detection gate, any secondary emission from an avalanche event in an array can propagate to the neighbor pixels and trigger false detections. If this crosstalk probability is not well controlled, the chain reaction can turn on the whole array with a single input photon and severely degrade the LADAR image quality. As the pixel pitch reduced from 100  $\mu\text{m}$  of the previously reported 32x32 GM APD arrays to 50  $\mu\text{m}$ , the crosstalk is an even greater concern. Several layers of proprietary isolation schemes were employed in the array design and process.

Figure 12 shows the 50  $\mu\text{m}$  pitch arrays demonstrating a crosstalk level about 60 ppm under the operation condition, which is about one order of magnitude less than that of the 100  $\mu\text{m}$  pitch 32x32 arrays we reported before<sup>4</sup>.

#### 4. LADAR SYSTEM FIELD TEST

Boeing DES developed a compact LADAR system based on the Spectrolab Gen-II 32x32 LADAR camera demonstrated above. The total weight is less than 20 lbs with the lens and scanning mechanics. The size is 990 cu. in., and the power consumption is less than 325W. With data reduction from hundreds of MB/s raw data to about 20 MB/s, this compact LADAR system gives the user rapid 3D imagery to access the mapped area quickly and accurately. At 1000 ft AGL, this system can cover 0.5 sq. mi/hour with a range resolution of 6 inches and a GSD of 5 inches. This system has been demonstrated on various ground and aerial platforms.



**Figure 13** The compact LADAR system integrated with the Spectrolab Gen-II LADAR camera by Boeing DES.

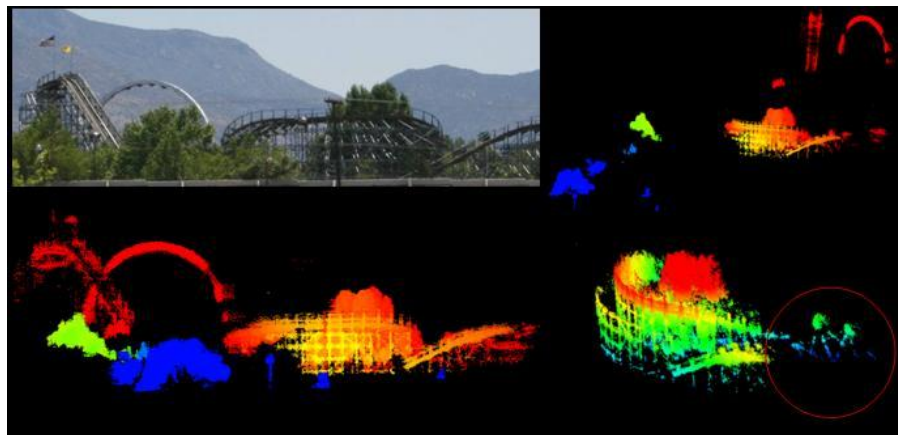


**Figure 14** Final static test of amusement park about 1000 ft away from Boeing-SVS office. The rotated image shows small Ferriswheel hidden in the view from the LADAR location.

As shown in Figure 14, the final ground static test demonstrated preparedness and highlights benefit of photon counting LADAR. The roller coaster clearly shows the depth even though the image was taken from one position. The rotated image shows small Ferris wheel hidden in the view from the LADAR location. Figure 15 shows another ground test for this LADAR system. At a distance about 300 m, the twigs and wires can be easily resolved.

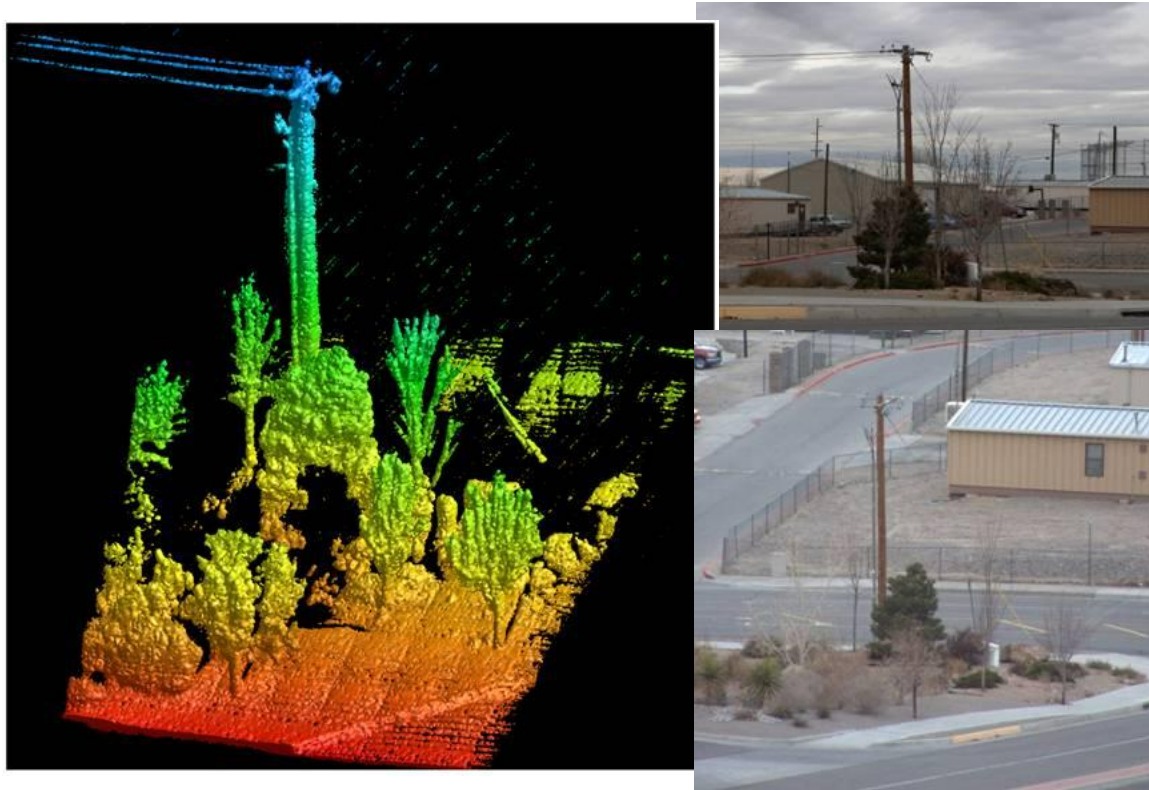


**Figure 15** LADAR system ground test with wires and trees at about 300m. The range is color coded.

Figure 16 shows the LADAR test system on a hot air balloon integrated with GPS/INU and battery power. Two different mounting positions are prepared for uncontrolled balloon landing and mounting to the wicker basket. The integration went smoothly with only minor issues with the GPS ground station at start-up. There are no hardware issues in the flight. The LADAR system was demonstrated on a hot air balloon platform. The flight took a little more than one hour, and the system collected over 30 minutes of data.

Figure 18 shows the 3D images of forested areas and the Rio Grande near Albuquerque, NM passed by in this flight. The images were taken at 1125 ft AGL and 11.5 mph, and the LADAR system scanned in a range of  $\pm 7^\circ$  at 2 Hz.

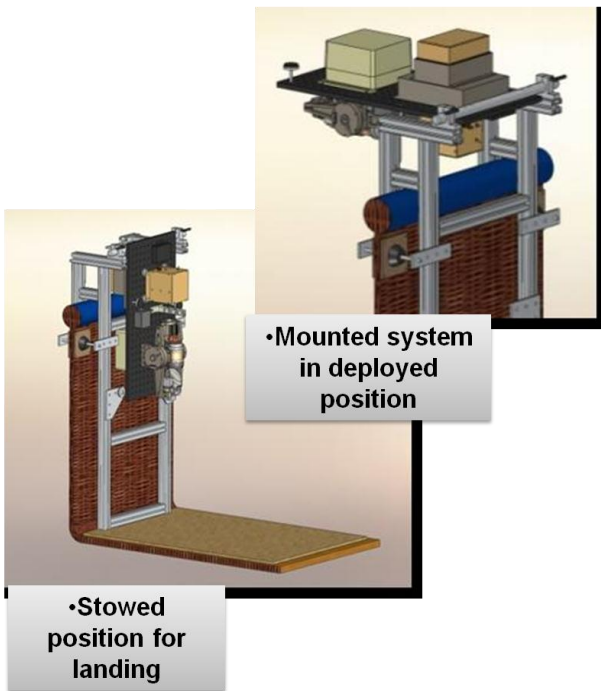


**Figure 16** Final LADAR test system on a hot air balloon integrated with GPS/INU and battery power.



**Figure 17** Hot air balloon demo on May 18, 2010.

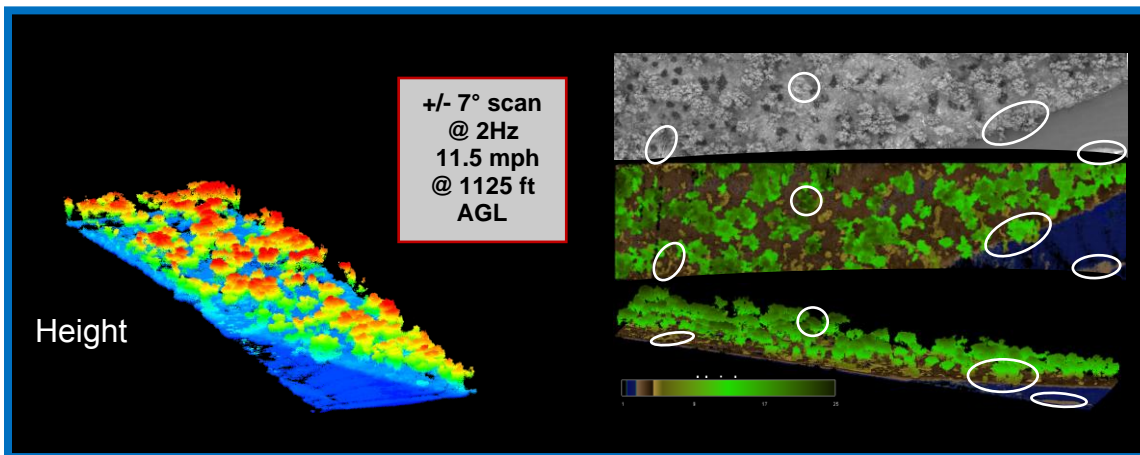


**Figure 18** 3D images of forested areas and the Rio Grande near Albuquerque, NM generated by a compact Boeing DES LADAR system mounted on a hot air balloon.

## 5. 32X128 GMAPD SCA

To answer the challenges of SWIR LADAR applications, Spectrolab, teamed with Boeing DES and Black Forest Engineering, developed a 32x128 GM-APD SCA as reported previously<sup>3</sup>. In order to suppress the crosstalk with 50  $\mu\text{m}$  pitch, half of that of the 32x32 array, an InGaAsP filter layer was inserted in the epitaxial structure to absorb the InP secondary emission. Based on this effort and the experience in our



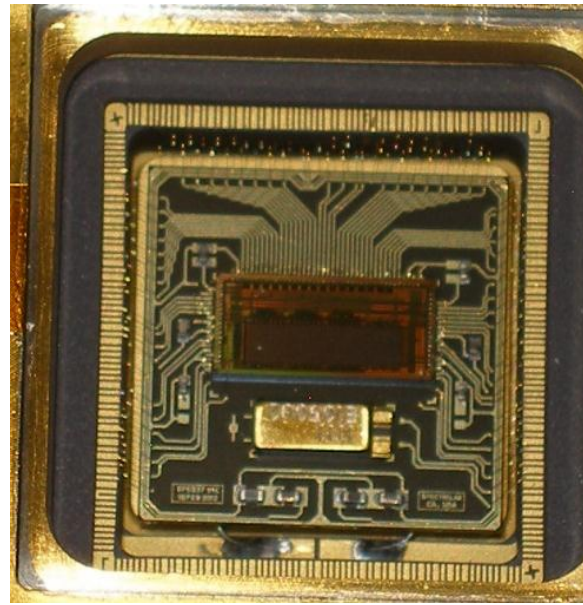
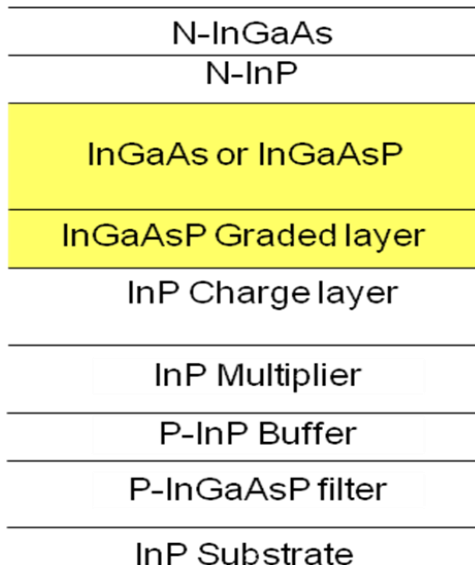


**Figure 20** The epitaxial structure for the 32x128 GM-APD array. An InGaAsP filter layer is inserted in the growth.

**Figure 19** The top view of 32x128 GmAPD SCA.

32x32 SCAs, the commercial 32x128 SCA has incorporated many new features, including full Cameralink control and output, 50 kHz frame rate at all gate width, 1000 m max range with programmable 0.3 ~ 1.0 ns bins, 14-bit timing resolution, short pixel protection, and 4-bit NUB correction. Although the size is four times of that of the 32x32 SCAs, the power consumption is kept at 600 mW, twice as much as the latest Gen-II 32x32 SCA. As shown in Figure 20, the FPA is located in the center of the SCA. Similar to the 32x32 SCAs, the final assembly will be hermetically sealed in a 160-pin PGA package with the same size and footprint. The cross section of the final SCA is shown in Figure 6. Based on this SCA development, the next generation GmAPD 32x128 LADAR camera will be demonstrated soon.

## 6. SUMMARY

For the SWIR LADAR applications, Spectrolab optimized the APD epitaxial design and device process and developed high performance 32x32 and 32x128 GmAPD image arrays and SCAs with 3-4 kHz DCR at 40% PDE, 60 ppm crosstalk at 50 μm pitch, 0.16V Vbr standard deviation, and no afterpulsing until 500 kHz frame rate. With many new features for manufacturability, operation stability and reliability, and application convenience, the Gen-II 32x32 GmAPD LADAR system has been demonstrated low SWAP footprint on various platforms with excellent resolution. For aerial mapping and reconnaissance application, a new 32x128 SCA and LADAR camera are under development.

## ACKNOWLEDGEMENTS

We would like to acknowledge the invaluable assistance provided by MIT Lincoln Laboratory and early stage funding from DARPA over the last several years under various technology transfer programs.

## REFERENCES

- <sup>1</sup> K. A. McIntosh, et al., "Arrays of III-V semiconductor Geiger-mode avalanche photodiodes," Lasers and Electro-Optics Society, 2003. LEOS 2003. The 16th Annual Meeting of the IEEE. Volume 2, 686 (2003).

- <sup>2</sup> R. Sudharsanan, et al., "Single photon counting Geiger Mode InGaAs(P)/InP avalanche photodiode arrays for 3D imaging," *Proc. SPIE* 6950, 69500N (2008).
- <sup>3</sup> P. Yuan, et al., "Geiger-mode LADAR cameras," *Proc. SPIE* 8037, 803712 (2011).
- <sup>4</sup> P. Yuan, et al., "32 x 32 Geiger-mode LADAR cameras," *SPIE Defense, Security, and Sensing, Laser Radar Technology and Applications XV. Proc. SPIE* 7684, 76840C (2010)